

Journal of Materials Chemistry A

Accepted Manuscript



This is an *Accepted Manuscript*, which has been through the Royal Society of Chemistry peer review process and has been accepted for publication.

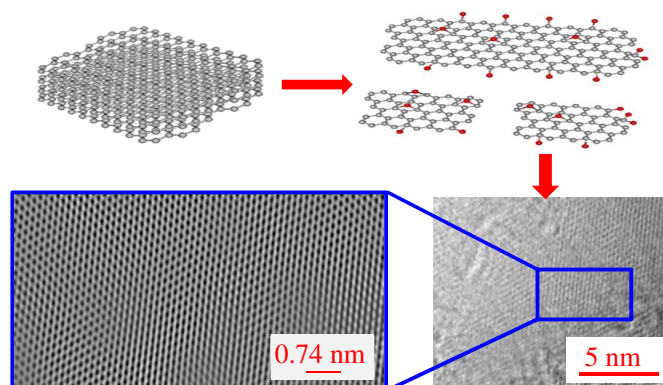
Accepted Manuscripts are published online shortly after acceptance, before technical editing, formatting and proof reading. Using this free service, authors can make their results available to the community, in citable form, before we publish the edited article. We will replace this *Accepted Manuscript* with the edited and formatted *Advance Article* as soon as it is available.

You can find more information about *Accepted Manuscripts* in the [Information for Authors](#).

Please note that technical editing may introduce minor changes to the text and/or graphics, which may alter content. The journal's standard [Terms & Conditions](#) and the [Ethical guidelines](#) still apply. In no event shall the Royal Society of Chemistry be held responsible for any errors or omissions in this *Accepted Manuscript* or any consequences arising from the use of any information it contains.

Graphical Abstract

Simultaneously oxidizing and ultrasonicing graphite for 60 min can create high-structural integrity yet solution-processable graphene for a great many applications.



ARTICLE

Advancement in Liquid Exfoliation of Graphite through Simultaneously Oxidizing and Ultrasonicing

Cite this: DOI: 10.1039/x0xx00000x

Ge Shi^{a,b}, Andrew Michelmore^b, Jian Jin^c, Luhua Li^d, Ying Chen^d, Lianzhou Wang^e, Fisher Yu^e, Gordon Wallace^f, Sanjeev Gambhir^f, Shenmin Zhu^g, Pejman Hojati-Talemi^b and Jun Ma^{*a,b}

Received 00th January 2012,

Accepted 00th January 2012

DOI: 10.1039/x0xx00000x

www.rsc.org/

Layered crystals, once exfoliated in liquids, create nanosheets with large surface area and likely generate electron band gaps. The current liquid exfoliation of graphite is performed by either oxidation, ultrasonication or the oxidation followed by ultrasonication; these methods are respectable but have limitations: the oxidation actually produces graphene oxide while the sonication is time-consuming with a low yield. In this paper we report a highly effective yet simple approach for the fabrication of high-quality graphene; the approach consists of simultaneously oxidizing and ultrasonicing graphite for merely 60 min, followed by washing and filtration. Exfoliation was markedly promoted by the simultaneous treatment, where 80% of the sheets comprise single or few layers with lateral dimensions ranging 50 nm to over 100 nm; their carbon to oxygen ratio is at 8.85; the ratio of Raman D- to G-band intensity is as low as 0.211; and the sheets can be stably dispersed in acetone for at least 48 hours and they have an electrical conductivity over 600 S/cm. A thin graphene film made by casting exhibited a *sheet resistance* of $\sim 1000 \Omega/\text{square}$ with 80% transparency at 550 nm.

1. Introduction

Layered materials are a class of substance that forms strong in-plane chemical bonds but displays weak out-of-plane, van der Waals bonds; these materials can be sheared parallel or expanded normal to the in-plane direction, producing nanosheets. A nanosheet consists of either a monolayer or less than 10 stacked monolayers.^{1,2} As the most extensively studied layered crystal, graphite can be converted to graphene by micromechanical exfoliation³, which cannot create processable graphene in solution because its product lacks sufficient functional groups and suitable lateral dimensions. Therefore, oxidization methods have been developed and widely used to produce graphene oxide.⁴⁻⁶ Graphene oxide is of very low electrical conductivity; reduction just mildly improves electrical conductivity, because it removes oxygen which takes carbon in the form of CO and CO₂ and subsequently creates additional new defects even while removing the "oxygen-associated" defects introduces earlier.⁷ The chemically reduced derivatives are actually limited by low electrical conductivity (<10 S/cm) with a risk of sacrificing its solution processability.^{8,9}

Three routes have been developed to obtain a large quantity of graphene, including: (i) liquid exfoliation of graphite by many-hour sonication,^{10,11} (ii) intercalation and expansion of graphite with volatile agents,^{12,13} and (iii) high-quality graphene platelets prepared by thermally expanding a commercial graphite intercalation compound (GIC) and subsequently ultrasonicing

the expanded product in a solvent.^{14,15} These methods have achieved decent success. However, the method (i) cannot produce monolayer graphene in high yield, the resulting sheets from (ii) and (iii) have insufficient surface functional groups for liquid processing, relatively high thicknesses (over 3 nm) and uncontrollable lateral dimensions. Therefore, it is of strategic importance to develop a one-step, scalable approach for the preparation of high-structural integrity yet solution-processable graphene.

We herein report a simple yet effective approach to produce high-quality graphene sheets by simultaneously oxidizing and ultrasonicing graphite within one hour. Although oxidization and ultrasonication are commonly used for the preparation of graphene oxide and graphene, the simultaneous treatment has never been reported. Whilst oxidization can introduce oxygen-containing groups to graphene sheets, ultrasonication at relatively low temperature is highly effective in exfoliating graphite platelets.¹⁵ Therefore, the simultaneous treatment – combining oxidization with ultrasonication (denoted as oxidisonication) for dozens of minutes – would be far more effective and efficient in producing single-layer and few-layer graphene than the current approaches. More importantly, the as-obtained graphene sheets feature high structural integrity with a moderate content of oxygen-containing groups. They show conductivity far higher than those of chemically reduced graphene oxide, and thus no reduction is needed for our graphene sheet. The sheets can suspend in water and other

solvents because of their oxygenated groups, and so a transparent conductive film can be readily obtained by casting.

2. Experimental

2.1 Materials

Graphite powder (Micro 0850) was provided by Asbury Carbons Pty Ltd. Potassium permanganate, sulphuric acid (95–98%) and phosphoric acid (85 wt%) were purchased from Sigma-Aldrich. Hydrogen peroxide (30 wt%) was bought from Chem-Supply.

2.2 Fabrication of graphene sheets

KMnO₄ (0.4 g) was dissolved in a mixture of concentrated H₂SO₄ (6.0 g) and H₃PO₄ (26.0 g). Graphite powder (0.1 g) was added into the mixture and stirred for 1 min. Then the mixture was immediately covered and placed into an ultrasonic bath (200 W and 42 kHz) for simultaneous oxidization and ultrasonication (oxidi-sonication). A cooler was connected with the bath to prevent heat build-up. During the oxidi-sonication, graphite flakes could exfoliate and split into graphene sheets; meanwhile, they were oxidized by Mn₂O₇ that was created by 2KMnO₄ (s) + H₂SO₄ (aq) → Mn₂O₇ (l) + K₂SO₄ + H₂O. The reaction can be terminated anytime by moving the mixture out of the bath and then adding 120 g water slowly, followed by vacuum filtrating and washing three times with water and hydrogen peroxide for removal of ions and acids. The prepared sheets should be stored in solvents such as water or acetone for the following film fabrication. For characterization in need of powder samples, the sheets were dried in an air-ventilated oven at 60°C and then in a vacuum oven at 100°C for 4 hours to remove crystalline water. Although we started with 0.1 g graphite, the product was weighed to be 0.105 g; the slight increment would be caused by the O element added by the oxidi-sonication and also likely due to the combined water.

2.3 Fabrication of graphene film

The as-prepared sheets were suspended in acetone by sonication of 10 min. Then the suspension (0.32 mg/mL in acetone) was carefully dropped on a glass slide that had been coated with polystyrene by plasma. After a number of droplets were added and slightly dried, the sheets would deposit on a desired area of the slide. After 60 s of drying which evaporated ~70 vol% acetone, the slide was placed on a spin coater and spun at 2,000 rpm for 30 s to obtain a film of relatively uniform thickness.

2.4 Characterization

X-ray diffraction (XRD) was performed using a diffraction technology mini-materials analyser (MMA). The diffractometer was equipped with curved graphite monochromators, tuned to Cu K α radiation (λ : 1.5419 Å) with a tube voltage applied at 35 kV and 28.2 mA (1 kW). The diffraction patterns were collected in a reflection mode geometry between $2\theta = 2\text{--}50^\circ$ at a scan rate of $1^\circ/\text{min}$.

XPS analysis was conducted by a SPECS SAGE XPS system with a Phoibos 150 analyser and an MCD-9 detector, which used non-monochromated Mg K radiation at 10 kV and 20 mA

(200 W). The analysis spot size was circular with a diameter of 3 mm.

Atomic force microscopy (AFM) micrographs were obtained by using a NT-MDT NTEGRA SPM instrument with NSG03 non-contact “golden” cantilevers. The magnitude of oscillation was 15 nm and the scan rate for $2\ \mu\text{m} \times 2\ \mu\text{m}$ images was typically 0.5 Hz. The samples were prepared by suspending the sheets in N-methyl-2-pyrrolidone (NMP) at 0.0004 wt% by 30-min ultrasonication below 30°C and then dropping the suspension on a silicon wafer followed by drying. A 100- μm scanner was used with calibration done by $1.5\ \mu\text{m}$ grids with a height of 22 nm. Raman spectra were recorded at room temperature by a Renishaw inVia Raman microspectrometer with 633 nm laser excitation and notch filters cutting at $\sim 100\ \text{cm}^{-1}$. Extreme care was taken to avoid sample damage or laser induced heating. Measurements were performed from ~ 4 to $\sim 0.04\ \text{mW}$ incident power.

The functional groups of graphene sheets were characterized using a Perkin-Elmer 65 FTIR spectrometer with a MIRacle single-reflection attenuated total reflectance (ATR) sample accessory. Thermogravimetric analysis (TGA) was performed on a TGA Q500 (TA instruments) at a heating rate of $10\ ^\circ\text{C}/\text{min}$ in N₂.

All the powder samples were pressed to produce sheets of below 0.5 mm in thickness by a bench top press YP-2 (Shanghai Shanyue Scientific Instrument Ltd) under a certain pressure to produce smooth surface. The sheet thickness was measured by a digital micrometre. The electrical conductivity of the sheets was examined with a Hall-effect measurement system with four probes that were tailor-made by the Platform for Characterization and Testing, Suzhou Institute of Nano-Tech and Nano-Bionics, the Chinese Academy of Sciences. In brief, four probes were located with intimate surface contact with a specimen, exactly at the four points of a square. After four current-voltage curves were measured to confirm the good contact between the probes and the specimen surface, resistivity testing was carried out under a resistance model. Electrical conductivity was calculated taking into account the sample geometry.

Micrographs of transmission electron microscopy (TEM) were obtained with a Philips CM200 at an accelerating voltage of 200 kV. The samples were prepared by suspending graphene sheets in THF at 0.0004 wt% by 0.5 hour sonication and then dropping the solution on 200-mesh copper grids, followed by drying. The bright-field high-magnification TEM images were taken from a JEOL 2100F microscope operated at 120 kV.

Visible light transmittance measurements were conducted on graphene films by a UV-Visible Spectrophotometer (Evolution 201 Computer Control Spectrophotometer 840-210800). The conductivity of graphene films was measured by a Four-Point Probing Measurement System (Keithley-4200, KeithLink Technology Co., Ltd) consisting of a bench top 4-point prober and a 4-point probe head for manual probing. Its supporting software measured the film resistance taking into account the sample geometry and thickness.

3. Result and discussion

3.1 Synthesis of graphene

We selected natural graphite powder as the precursor, a mixture of sulphuric acid and potassium permanganate as the oxidants, and phosphoric acid as the buffer solvent. These ingredients

were mixed in a glass beaker which was then immediately placed into a sonic bath to simultaneously undertake oxidation and ultrasonication (oxidi-sonication) (Fig. 1a and Fig. S1). As low-temperature ultrasonication proved effective in splitting graphite,¹⁵ the bath was preferably connected with a cooler. After 60 min oxidi-sonication, the product was repeatedly washed through vacuum filtration. Our product graphene sheets can suspend in acetone (0.1 mg/ml) for at least 48 h (Fig. 1b), and this suspension can be utilized to fabricate a highly transparent film (Fig. 1c) whose preparation, structure and properties will be discussed later in this work.

The mechanism of oxidi-sonication is depicted in Fig. 1d. Firstly potassium permanganate reacted with sulphuric acid to form Mn_2O_7 that oxidized graphite.^{16,17} Since the reaction

occurred at low temperature ($\sim 1^\circ C$) in a moderate environment containing a lot phosphoric acid, the speed of forming Mn_2O_7 was low (Fig. S2 a1–2), and this combining with the short oxidation time – 60 mins – contributes to a low degree of oxidation (Fig. S2 a3), implying high structural integrity for the product. This means that our method may eliminate the need of reduction required for graphene oxide. Facility requirements were also simplified since there was no toxic gas evaporation. The oxidation by Mn_2O_7 could initially occur at the graphene edges,^{18,19} which, assisted by the simultaneous ultrasonication, should increase electrostatic repulsion leading to more efficient exfoliation.

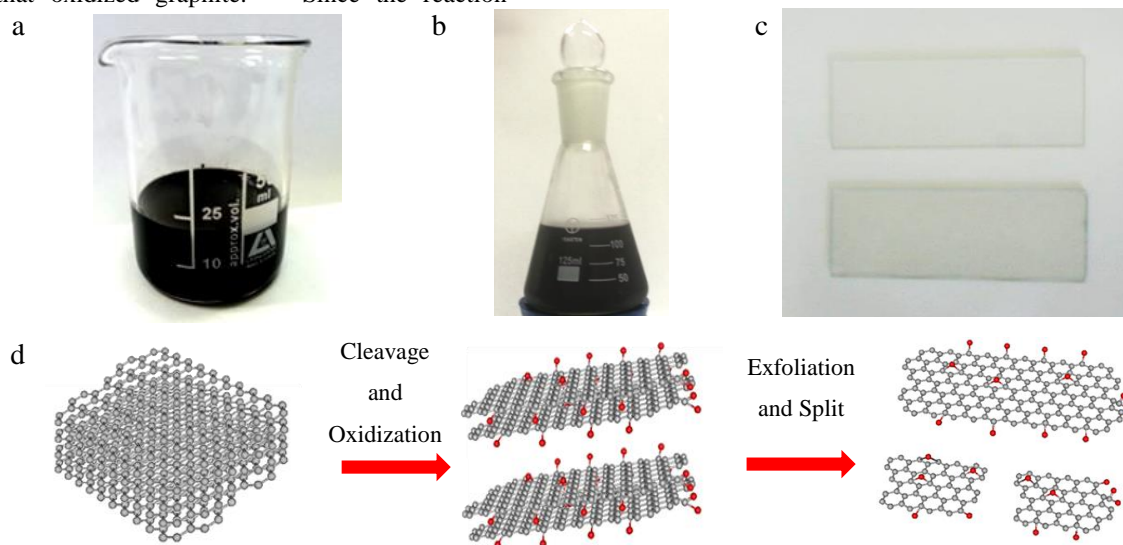


Fig. 1 Schematic for simultaneously oxidizing and ultrasonating (oxidi-sonication): (a) a front view of the beaker, (b) aqueous graphene suspension stable for at least 4 hours, (c) uncoated (top) and coated (bottom) glass slides, and (d) illustration of graphene synthesis.

To elaborate the effectiveness of the simultaneous treatment, a number of control experiments were designed and conducted. We produced three samples respectively by treating graphite 60 mins with (i) oxidation only, (ii) ultrasonication only and (iii) simultaneous oxidation and ultrasonication. Figs. 2a–d contain AFM micrographs and height profiles of these samples. Whilst raw graphite particles are as high as 85 nm, the sheets made by the oxidi-sonication (~ 1.0 nm) are far thinner than those by either oxidation (~ 70 nm) or ultrasonication (~ 10 nm). During the simultaneous treatment, more and more oxygen-containing groups were produced on graphene plane causing defective sites, and this would help ultrasonication to chop large graphene sheets (500 nm) into smaller ones. Therefore, oxidation and ultrasonication promoted each other when conducted simultaneously, which efficiently reduced the fabrication time (only 60 mins) while maintaining the high structural integrity of graphene plane. *It is worth noting that our oxidi-sonication method produces graphene sheets of various thickness values. By randomly selecting 72 sheets, the thickness was measured as 0.85 ± 0.10 nm in one of our many studies for this work. Fig 2d shows the thickness of a sheet which is close to the average value.*

The thickness and lateral dimension of graphene sheets are critical to applications. Fig. 3a contains the statistics for 70 pieces of randomly selected graphene sheets from AFM observation; of these, over 80% sheets consist of 1 to 3 layers having an average lateral dimension of 75 ± 25 nm, with a monolayer graphene yield of $\sim 44\%$ as a dominant composition. Fig. 3b shows the distribution of lateral dimension/thickness ratios calculated from randomly selected 25 sheets, and the lateral dimension statistics are available in Fig. 3c which shows there are indeed a number of large sheets. A large number of graphene sheets having similar lateral dimensions and thicknesses can be observed at low magnification AFM micrographs (Fig. S3c and d). The low lateral dimension would provide graphene sheets with higher surface charge density, resulting in higher electrostatic forces preventing the sheets stacking; these sheets have potential to reinforce and toughen polymers.

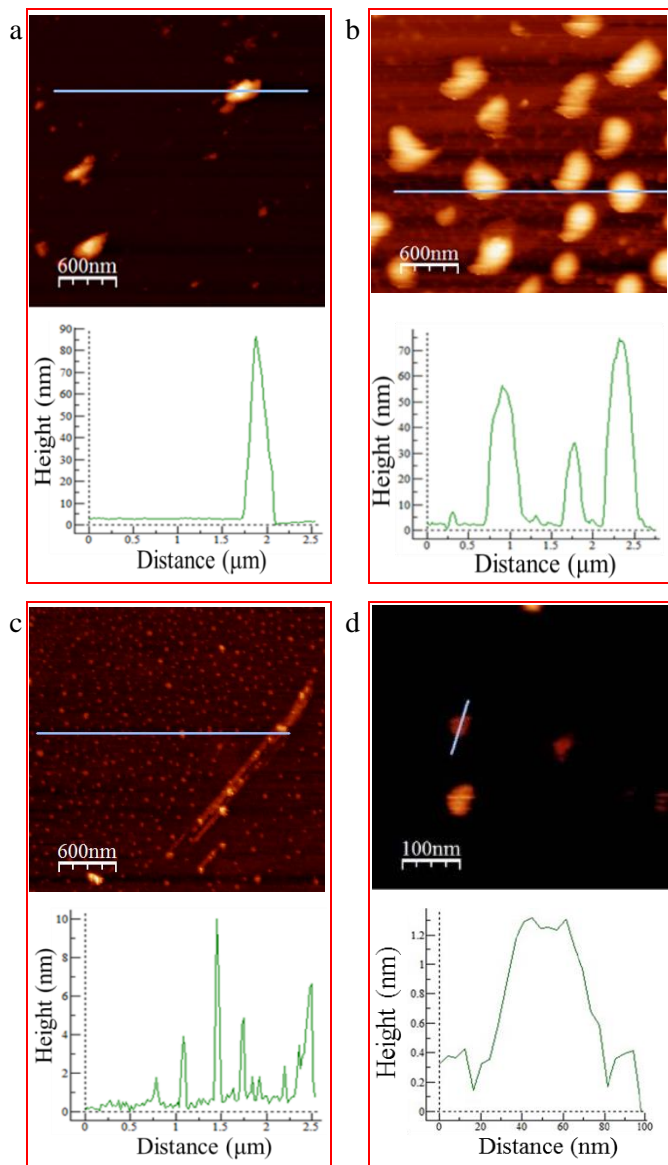


Fig. 2 AFM micrographs and height profiles of (a) raw graphite particles, ~90 nm in thickness and ~500 nm in lateral dimension, (b) product by 60 minutes of oxidization only, ~70 nm and ~500 nm, (c) 60 mins of ultrasonication only, ~10 nm and ~150 nm, and (d) 60 mins of oxidization, ~0.9 nm and ~60 nm.

^aSchool of Engineering

^bMawson Institute, University of South Australia, SA5095, Australia.

^cSuzhou Institute o

^dNano-Tech and Nano-Bionics, Chinese Academy of Sciences, Suzhou 215123, China

^eInstitute for Frontier Materials, Deakin University, Geelong Waurn Ponds Campus, VIC 3216, Australia

^fSchool of Chemical Engineering and AIBN, the University of Queensland, QLD 4072, Australia

^gIntelligent Polymer Research Institute, University of Wollongong, NSW 2500, Australia

^hState Key Laboratory of Metal Matrix Composites, Shanghai Jiao Tong University, 200240, China

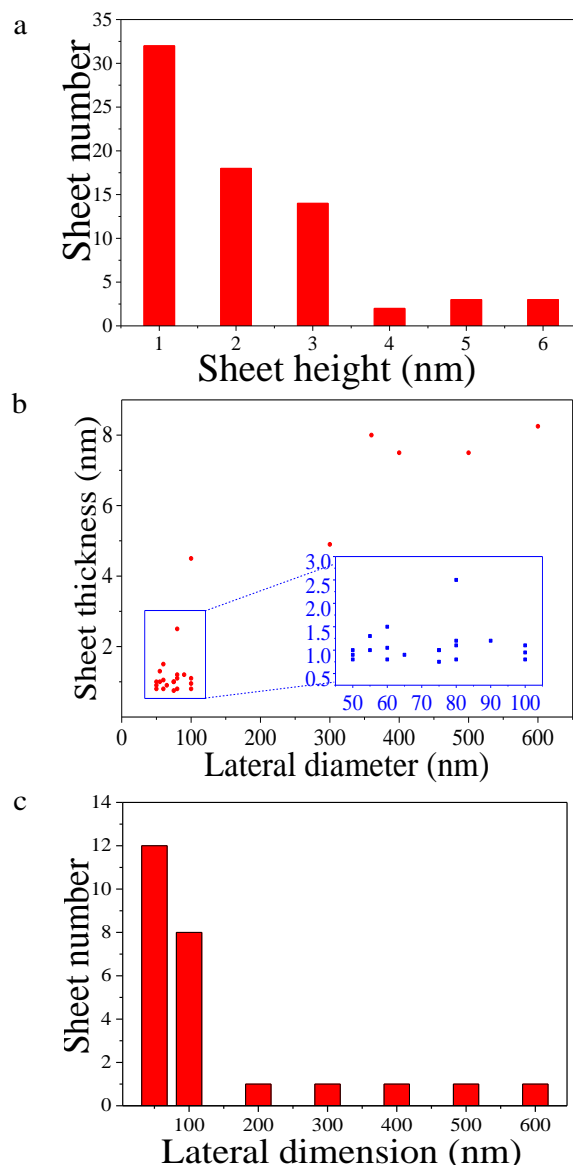


Fig. 3 (a) Histogram of graphene sheets by 60-min oxidi-sonication, (b) sheet thicknesses versus lateral dimension and (c) histogram of the sheet number versus lateral dimension.

3.2 Crystal Structure of graphene

Fig. 4a and b show bright-field TEM micrographs of two large graphene sheets made by the oxidi-sonication of 60 min; the large sheets were selected due to the need of selected area electron diffraction (SAED), which was conducted on randomly selected regions of these sheets along the [001] zone axis. The SAED patterns (Fig. 4e and f) exhibit typical six-fold symmetry, in consistence with the hexagonal crystalline structure of graphene sheet. The well-defined diffraction pattern (Fig. 4e) confirms the crystalline structure of a single-layer graphene. According the measurements of diffraction peak intensity (Fig. 4e and f), the diffraction intensity ratios between {1100} and {2110}¹⁸ spots are ~3.5 and 0.5 respectively for single and double layer graphene. The observed contrast of intensity confirms the presence of single and double layer graphene.²⁰⁻²²

All of these techniques unequivocally show that high-crystalline graphene sheets have been produced through the 60-min oxidi-sonication.

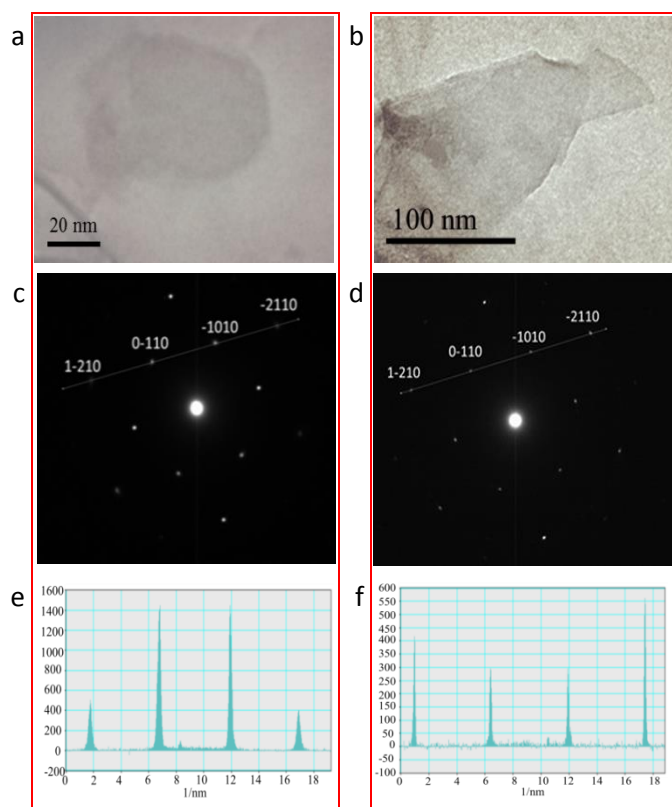


Fig. 4 TEM images of graphene sheets made by 60-min oxidi-sonication: (a) monolayer graphene and (b) bilayer graphene, electron diffraction patterns (c) and (d) respectively taken from (a) and (b) with the peaks labelled by Miller-Bravais indices, and diffraction intensity of (e) single-layer graphene and (f) double-layer graphene taken along the 1–210 to –2110 axis.

Fig. 5 illustrates high-resolution TEM micrographs of a typical graphene sheet. Although some regions have defects in nanoscale as indicated by dark blue arrows, the most area of graphene sheet has intact crystalline structure. The defective regions rich in hydrophilic oxygenated groups can improve the dispersibility in water or polar organic solvents, while the crystalline regions maintain high electrical conductivity of graphene. The right image in Figure 5a shows a FFT-filtered TEM image from part of the left image. In specific, part of the left TEM image was chosen and FFT-transferred. Then a Fourier mask was applied to the FFT image before the image was transferred back to a normal TEM image at atomic resolution. Thus, our graphene sheets would be a promising precursor for the fabrication of transparent and conducting films by casting, as to be discussed later.

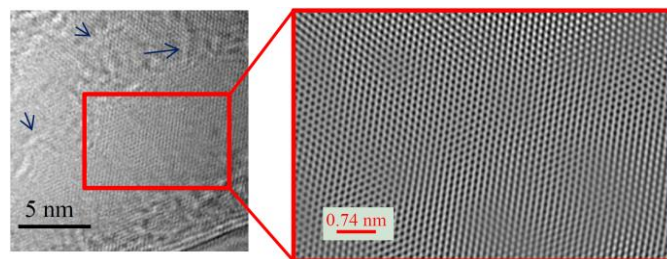


Fig. 5 High-magnification TEM micrograph of a typical graphene sheet

3.3 Evolution of graphene during oxidi-sonication

It is now indispensable to combine oxidization with ultrasonication (oxidi-sonication) for the fabrication of cost-effective, low-defect, solution-processable graphene sheets. The time of oxidi-sonication also plays a critical role in determining the thickness, size and oxidization degree of graphene sheets. We found that the fraction of the single and few layer sheets increases obviously with the oxidi-sonication time (Fig. 6a1, b1 and c1). The graphene sheets obtained at 20, 40 and 60 mins were respectively measured to be ~7 nm, ~3 nm and ~1 nm in thickness; and the lateral dimensions were ~1000 nm, ~100 nm and ~50 nm. Representative sheet morphology and profiles are shown in Fig 6a2–3, b2–3 and c2–3. With increase in the treatment time, the oxidi-sonication produced more oxygen-containing groups and this weakened the interlayer interactions, resulting in the effective exfoliation.

X-ray diffraction (XRD) (Fig. 7a) analysis was performed to investigate the evolution of graphite in this process. All samples have two diffractions at ~26.5° and ~25.3°, implying a potential structural change caused by the oxidi-sonication.²³ The graphite's diffraction pattern at 26.5° is well known and thus omitted here. The diffraction at ~25.3° refers to a larger spacing at ~0.36 nm. It is noteworthy that both diffractions are broad in comparison with the sharp diffraction of raw graphite which has been shown by many studies. The broadness may indicate that the simultaneous sonication and oxidation (oxidi-sonication) is powerful to change the layered structure of graphite while maintaining high structural integrity. With increase in the processing time, the diffraction intensity at 25.3° increases, indicating the layer spacing expanded by the treatment. Two relatively broad patterns of mild intensity are observed for the sample made by the 20-min oxidi-sonication, where oxygen-containing groups produced might bond to the edges of basal planes of the graphite structure. These functional groups may slightly expand the interlayer distance of graphene sheets. Due to the low degree of oxidization, only few domains of graphene layers would be oxidized. Actually the usual 7.5° diffraction line of graphene oxide is not shown, and the diffraction pattern at 26.5° implies a high degree of crystallinity.^{24,25}

As the oxidi-sonication time increases to 40 min, the diffraction intensity at 26.5° reduces while it increases at 25.3°, reflecting an increase in the layer spacing of graphite. A further increase to 60 mins leads to decline in both diffraction intensity, because

of a larger quantity of functional groups generated that interacted with water molecules thus loosening the stacking of graphene layers.²⁶ Since all samples were tested in their powder

form where the sheets stacked, the diffraction patterns are substantially different to that of single layer graphene.²⁷

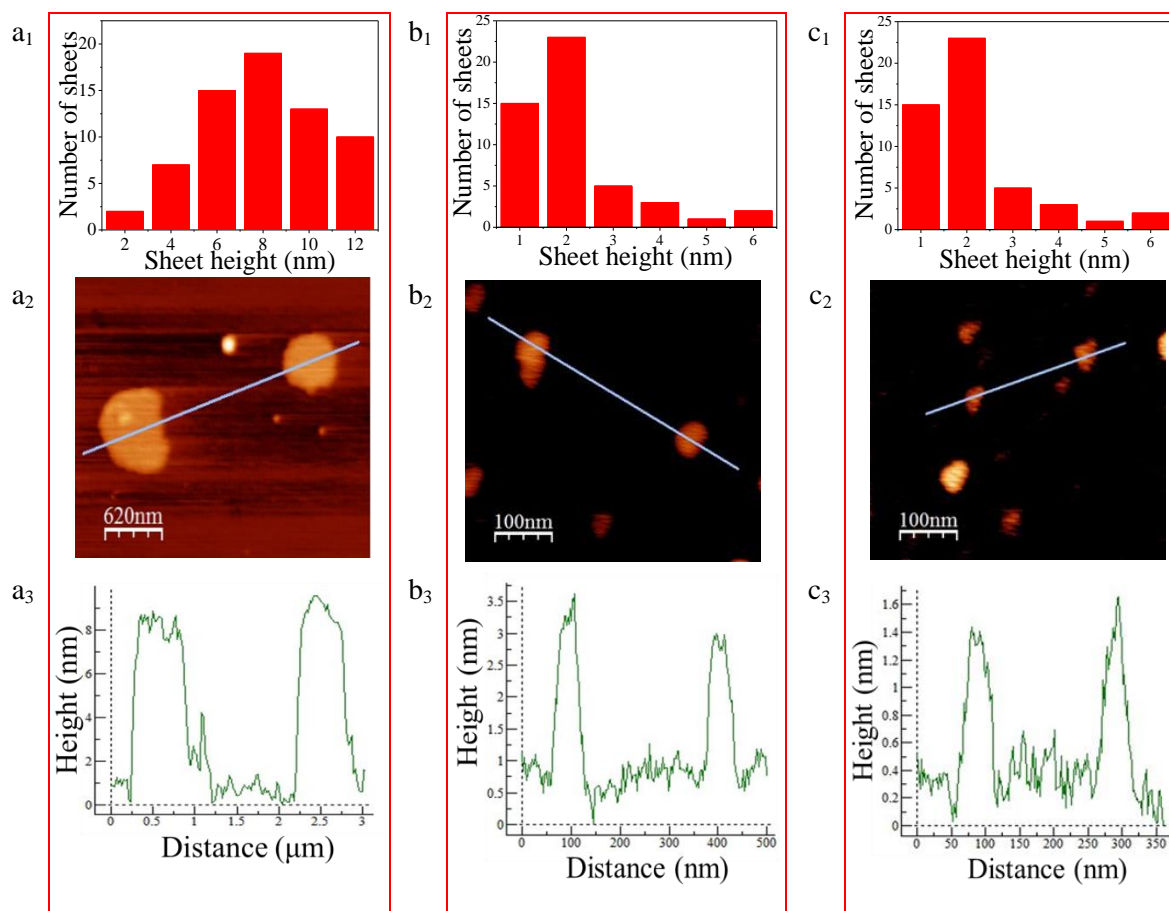


Fig. 6 Statistics and AFM micrographs and height profiles of graphene sheets made by oxidi-sonication for 20 mins (a1–3), 40 mins (b1–3) and 60 mins (c1–3).

Although Raman spectra were collected from the powder form of the samples, it is able to probe the evolution of sheet structure during oxidi-sonication. In Fig. 7b, all samples show peaks at around 1340, 1585 and 2690 cm^{-1} , and they are respectively assigned to the D, G and 2D bands of carbon.²⁸ G peak refers to sp^2 resonance on an ordered graphitic lattice, and D peak is activated from the first-order scattering process of sp^2 carbons by the presence of substitutional in-plane hetero-atoms, vacancies, grain boundaries or other defects, which might be sp^3 . The D peak intensity increases as the oxidi-sonication proceeds, signifying an increase of the aforementioned defects, because (i) the oxidization caused sp^3 hybridized carbon and (ii) as large graphite flakes were split into many small graphene sheets, there were more sheet edges leading to more disordered structure and lower symmetry.^{29,30} The increase in the oxidi-sonication time makes the shape of G peak unsymmetrical—the shoulder peak in G (1605 cm^{-1}) increases slightly as the oxidi-sonication proceeds; this is likely caused by the sheet lateral size reduction, as supported by a previous study where smaller lateral dimension of graphene made G peak unsymmetrical.^{28,29,31} The D to G ratio increases from 0.106 for the 20 min oxidi-sonication to 0.211 for the 60

min one. Nevertheless, this ratio is much lower than those for reduced graphene oxide in many previous studies,^{32,33} confirming the high structural integrity of our graphene. This may imply that any forms of reduction may not be necessary to further improve our graphene integrity.

Since both shape and wave number of the 2D peak are dependent on the number of graphene layers, they can be used to distinguish the layered structure of graphene.^{32,34} With reduction in the layer number for each sheet, the broad 2D peak would gradually converge to a line shape for single-layer graphene,³⁵ as explained by the evolution of electronic bond structure of graphene according to the double resonance theory.³⁵ The calculation of G to 2D intensity ratio can be used to conveniently estimate the number of graphene layers.^{36,37} Each of the three samples exhibits a strong 2D peak at 2600–2775 cm^{-1} , because they consist of graphitic sp^2 carbon structure. With increase in the oxidi-sonication time from 20 to 60 min, the 2D peak appears sharper and more asymmetric, it shifts from 2720 to 2695 cm^{-1} , and the G to 2D ratio decreases from 1.398 to 1.134 (Fig. 7c). All these changes are explained by a fact that with increase in the oxidi-sonication time, more

few-layer and monolayer graphene sheets were produced. The decrease of half maximum widths of 2D peaks from 75 to 65 cm^{-1} also indicates a lower quantity of large graphitic sheets left in the sample after 60-min oxidi-sonication, as supported by a previous research.^{38–40}

Fourier transform infrared spectroscopy (FTIR), thermogravimetric (TGA) analysis and X-ray photoelectron spectroscopy (XPS) were employed to probe the chemical composition of our products at different stages of the oxidi-sonication. The FTIR spectra (Fig. 7d) recorded the presence of hydroxyl groups (3400 cm^{-1}), carboxyl groups (1650 cm^{-1}), C=C from unoxidized $2p^2$ C–C bonds (1600 cm^{-1}) and epoxide and ether groups (1250 cm^{-1}). As the oxidi-sonication proceeds from 20 to 60 mins, the absorption intensity at 1250 cm^{-1} increases implying more epoxy and ether groups formed. The C/O ratio was determined from the C1s ($\sim 286\text{ eV}$) core level spectra (Fig. 7e). The 60-min product shows a C/O ratio of 8.85 far higher than the ratios reported for graphene oxide.^{41–46} In Fig. 7e, the fitted peaks occurring at about 284.2, 286.2 and 289.8 eV usually correspond to the unoxidized sp^2 C=C bonds, hydroxyl or epoxide groups (C–OH or C–O–C) and carboxyl groups (C=O). The evolution of FTIR and XPS spectra means that the surface functionality of our graphene sheets can be manipulated by adjusting the oxidi-sonication time. The increase in quantity of the functional groups led to stronger acid functionality, which was proved by the decrease in the Equivalence point from 9.0 (20-min oxidi-sonication) to 6.6 (60-min) for the 0.1 M NaOH solution by titration (Fig. S4).

TGA data (Fig. 7f) indicates a mass loss below $100\text{ }^\circ\text{C}$ owing to the removal of adsorbed water.⁴⁷ Of the three samples, the 60-min graphene indicates the largest weight loss from 25 to $100\text{ }^\circ\text{C}$ because the longest oxidi-sonication time produced the largest quantity of hydrophilic groups which absorbed water molecules. A major weight loss occurs from ~ 200 to $500\text{ }^\circ\text{C}$ for each sample corresponding to the escape of CO and CO_2 , both of which were produced from the oxygen-containing functional groups such as hydroxide and carbonyl groups.¹⁶ In comparison with graphene oxide (GO) that shows an abrupt weight loss (60%–90%) between 150 to $500\text{ }^\circ\text{C}$,^{48,49} our graphene sheets exhibit *no massive* weight loss ($\sim 10\%$) in the same temperature range, indicating a higher thermal stability (Fig. S5).

Since our graphene sheets have high structural integrity and low oxidation degree, we proceeded to the measurement of electrical conductivity. We first made graphene papers ($\sim 0.1\text{ mm}$ thick) from graphene sheets respectively by the 40 mins and the 60 mins of oxidi-sonication, and their electrical conductivity values were measured to be 820 and 679 S/cm. Notably, these values are much higher than those GO and reduced GO papers (from 0.8 to 374 S/cm).^{50–53} Therefore, as mentioned earlier in this study, any forms of reduction are not necessary to our graphene sheets.

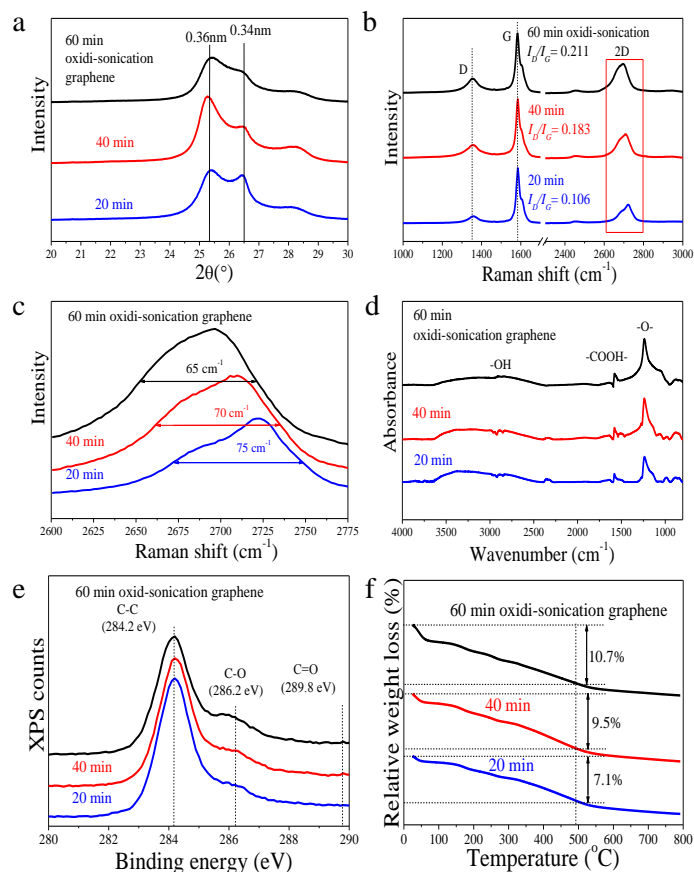


Fig. 7 Identification of chemical composition of graphene produced by oxidi-sonication: (a) XRD spectra, (b) Raman spectra, (c) 2D bands in (b), (d) FTIR, (e) XPS and (f) TGA plots.

3.4 Graphene thin film

We prepared transparent conductive graphene films by casting—dropping graphene/acetone suspension ($\sim 0.32\text{ mg/ml}$) onto a polystyrene-coated glass slide. The preparation mechanism is depicted in Fig. 8. Prior to casting, ultrasonication was used to obtain the uniform suspension of graphene sheets. As discussed in Section 3.3, the edges of the graphene sheets contain functional groups giving rise to molecular interaction that connects graphene sheets edge by edge; this can result in strong electrostatic repulsion and thus prevents the sheets overlapping.²⁶ The low lateral dimensions ($50\text{--}100\text{ nm}$ for most sheets), favouring the formation of strong electrostatic and solvation forces, also prevent graphene stacking (see the rectangle in Fig. 8a3). Therefore, during evaporation where the sheet concentration increases, the sheets may lay themselves edge by edge rather than stacking, forming nanoribbon-like structure (rectangle in Fig. 8b3). As acetone evaporates, these graphene sheets via $\pi\text{--}\pi$ interaction attach with the substrate coated with polystyrene by plasma. Graphene sheets in the subsequent casting would attach either on the polystyrene coating or with these pre-attached ribbons to form stacking. The graphene sheets may form island-like structure with height up to 20 nm (rectangle in Fig. 8c3). The subsequent

30-second spin coating would eliminate large overlapping particles and thus homogenizes the sheet distribution (Support Information Section 5). Taking advantage of the low oxidization and high solution processability of our graphene, this thin-film fabrication method has the following advantages: (i) one-step reaction without additional modification or

reduction,⁵⁴ (ii) the homogeneity and thickness of the film could be simply determined by the content of parent suspension and spin coating parameters (speed and duration), (iii) inexpensive fabrication devices and starting materials and (iv) high yield and short processing time (~2 min).

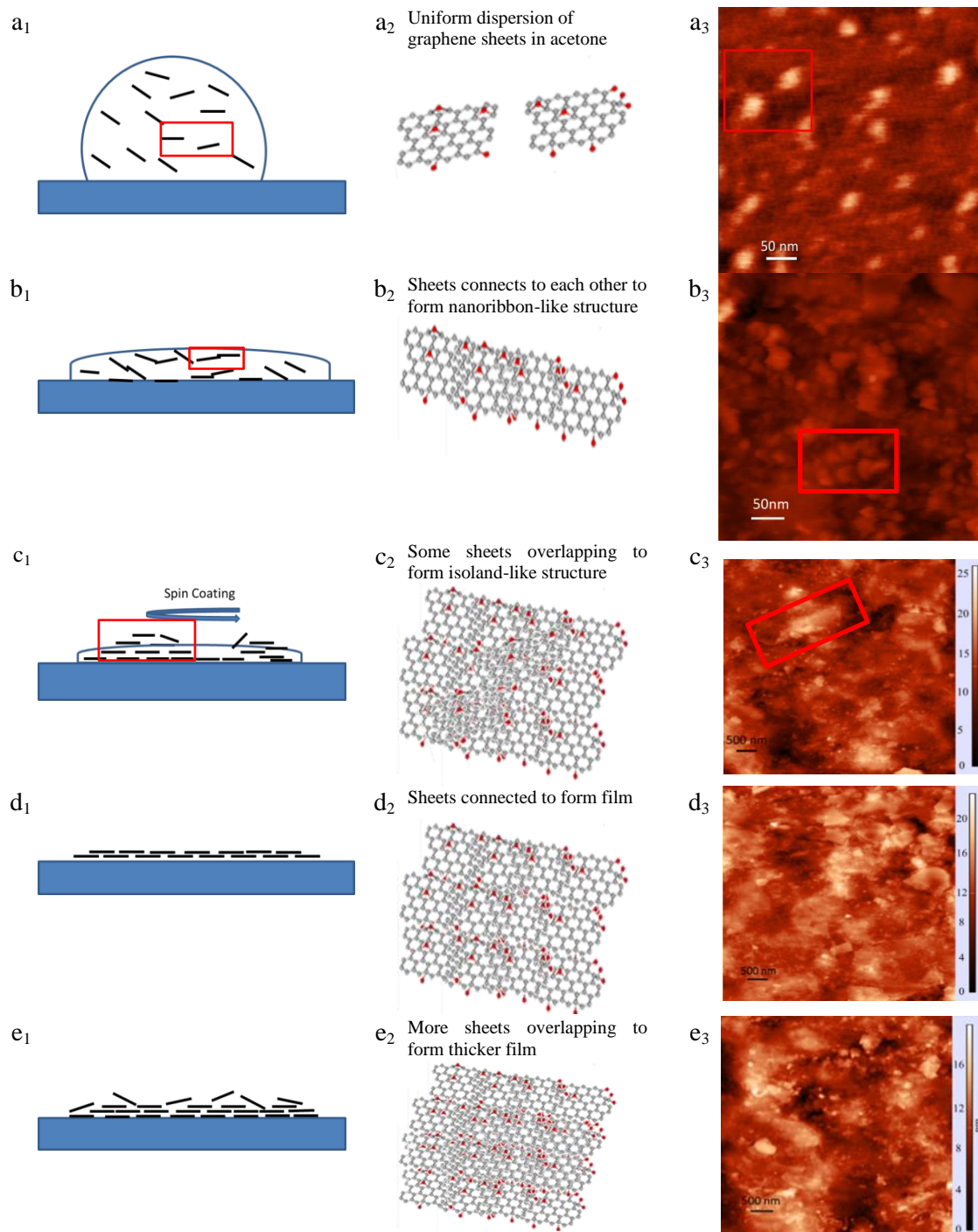


Fig. 8 Schematic for the fabrication of graphene film: (a1–3) graphene sheets disperse in acetone on substrate; (b1–3) as acetone evaporates, the sheets connect with each other producing ribbon-like structure; (c1–3) through partial evaporation, some of the randomly assembled graphene sheets can form island-like structure of 5–10 nm in height; (d1–3) after spin coating, the graphene sheets connect each other to form a graphene film of 3–5 nm in thickness; (e1–3) with increase in the sheet quantity, a 5–10 nm thick graphene film forms.

The morphology of a graphene film mainly depends on (i) the thickness of graphene sheets; (ii) the sheet distribution on substrate and (iii) the surface roughness of substrate (~15 nm in this case) (Fig. S6). We manipulated the film thickness by adjusting either the droplet numbers or the concentration of graphene suspension. We used light transmittance and AFM micrographs to estimate the average thickness of these films. In Fig. 8 d3 and e3, light colour could correspond to the regions covered by graphene sheets, while dark colour may refer to the regions uncovered; these transparent graphene films have relative flat surface and thickness below 10 nm. Albeit the existence of the uncovered domains, graphene sheets connect with each other edge by edge as shown in the rectangles in Fig. 8b and c.

The optical and electrical properties of graphene films of 7.5×2.5 cm² in lateral size were measured by an ultraviolet-visible spectrometer and a four-probe meter. In the visible range, the films show transmittance of 96%, 92% and 87% (Fig. 9a), which respectively should contain in average 1–2, 3–4 and 5–6 layers, by assuming our low-oxidation graphene having a similar optical absorption to that (2.3%) of single-layer graphene.^{55,56} In brief, we found that the thickness or transparency of graphene thin films can be controlled by changing the number of graphene suspension droplets, thus paving the way of liquid phase graphene coating for various applications.

The film contact angles were measured to be 25.2 – 75.3° by wettability measurement using water droplets (Fig. 9a), indicating an enhancement of surface hydrophobicity with increase in the graphene layers. When a water droplet adsorbs on a flat glass substrate, complete wetting occurs and the contact angle could be 0°. Due to the prevailing C–C and C=C bonds in graphene, the graphene film is slightly hydrophobic, and this disrupts the dynamic hydrogen bonds of water, resulting in translational and rotational entropy loss of water molecules. As a result, water molecules tend to migrate away from the gap between water and graphene.²⁶ With increase in the number of graphene layers, the surface energy decreases, the contact angle increases correspondingly, and thus the film surface becomes more hydrophobic the contact angle increases correspondingly, and thus the film surface becomes more hydrophobic.

Since a single-layer graphene film usually has higher resistivity to electrical current than stacked multilayers (3–8 layers) graphene film,^{33,57} we measured the *sheet resistance* of multilayer graphene films by a four-probe method (Fig. S7). In

Fig. 9b, the average *sheet resistance* values of graphene films are in the range of 1910 to 340 Ω/square (Fig. 9b), 10–500% lower than those of the thin films made from graphene oxide with tedious chemical^{58,59} or electrochemical reduction.¹⁸ It is worth to point out that our films were simply prepared through one-step casting where reduction is not necessary due to the high structural integrity of our graphene sheet (C/O ratio at 8.85 and Raman $I_D/I_G=0.211$ in Fig. 7b). The high sheet conductivity can be explained as follows: (i) the graphene sheets made by the oxidi-sonication have high conductivity; (ii) the spin coating effectively spread graphene sheets; and (iii) the interaction with polystyrene separated the aggregation of sheets. The film conductivity enhances from 54 to 280 S/cm as the thickness increases (Fig. 9c). The main reason for the low resistivity of our films is that oxidization and ultrasonication supported each other, leading to efficient exfoliation of graphene sheets at a low oxidation degree. In comparison, the conventional oxidation method is in need of a far longer oxidization time with much stronger oxidization agents; as a result, heavily oxidized graphene sheets with many structural defects are produced, and only a part of these defects can be amended by reduction. *Therefore, the oxidi-sonication graphene films possess higher optical-electrical properties than other transparent graphene films consisting reduced GO (supporting information section 9).* The current–voltage measurements of films were performed at room temperature as shown in Fig. S8a, and the results are presented in Fig. S8b.

As an old saying “Every coin has two sides”, our graphene sheets feature low thickness, high structural integrity and facile processability in solution, but their low lateral dimensions cause relatively high inter sheet contact resistance. This explains our sheet-film resistances (1910–340 Ω/square) similar to those consisting of ultra large GO sheets (1500–400 Ω/square).⁶⁰⁻⁶²

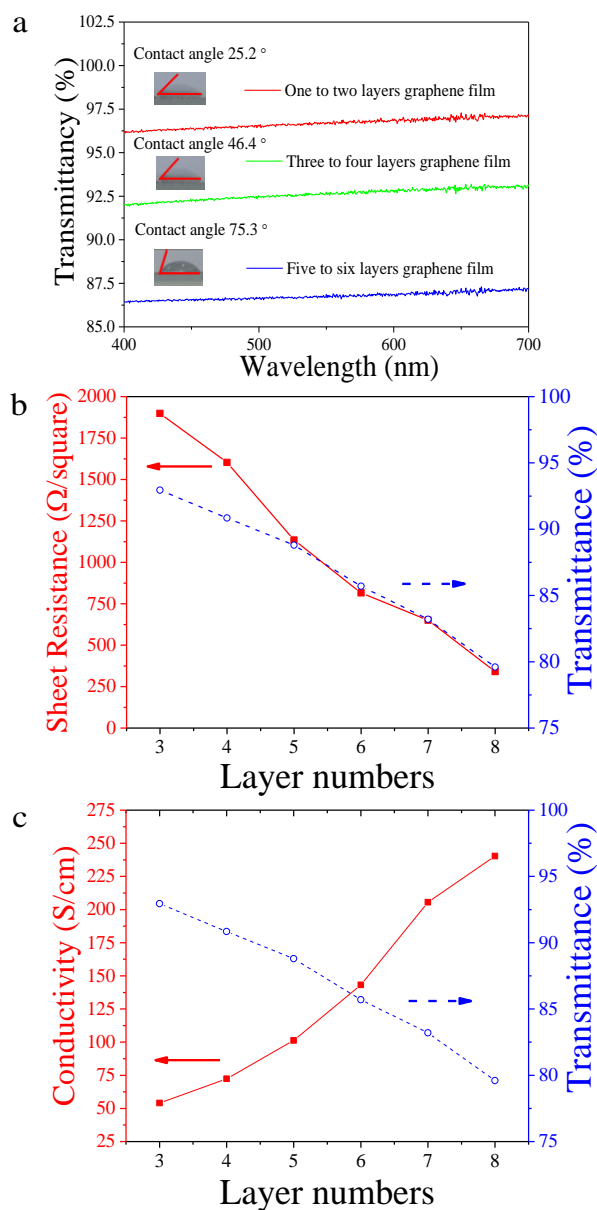


Fig. 9 (a) visible light transmittance spectra of graphene films, with insets showing H₂O contact angle, (b) the sheet resistance and (c) the conductivity of graphene films versus transmittance of 550 nm visible light.

Notes and references

- V. Nicolosi, M. Chhowalla, M. G. Kanatzidis, M. S. Strano and J. N. Coleman, *Science*, 2013, **340**, 1226419.
- N. Saber, S. Araby, Q. Meng, H. Y. Hsu, C. Yan, S. Azari, S. H. Lee, Y. Xu, J. Ma and S. Yu, *Nanotechnology*, 2014, **25**, 045501.
- Y. Zhu, S. Murali, W. Cai, X. Li, J. W. Suk, J. R. Potts and R. S. Ruoff, *Adv. Mater.*, 2010, **22**, 3906–3924.
- M. He, J. Jung, F. Qiu and Z. Lin, *J. Mater. Chem.*, 2012, **22**, 24254–24264.
- B. C. Brodie, *Philosophical Transactions of the Royal Society of London*, 1859, **149**, 249–259.
- W. S. Hummers and R. E. Offeman, *J. Am. Chem. Soc.*, 1958, **80**, 1339.
- L. Wang, X. Lu, S. Lei and Y. Song, *J. Mater. Chem A*, 2014, **2**, 4491–4509.
- S. Park and R. S. Ruoff, *Nat Nano*, 2009, **4**, 217–224.
- I. K. Moon, J. Lee, R. S. Ruoff and H. Lee, *Nat Commun*, 2010, **1**, 73.
- A. A. Green and M. C. Hersam, *Nano. Lett.*, 2009, **9**, 4031–4036.
- V. C. Tung, M. J. Allen, Y. Yang and R. B. Kaner, *Nat Nano*, 2009, **4**, 25–29.
- M. Pykal, K. Šafářová, K. Machalová Šišková, P. Jurečka, A. B. Bourlinos, R. Zbořil and M. Otyepka, *J. Phy. Chem C*, 2013, **117**, 11800–11803.
- M. Cai, D. Thorpe, D. H. Adamson and H. C. Schniepp, *J. Mater. Chem.*, 2012, **22**, 24992–25002.

Conclusions

We developed a simple, one-step method for the preparation of processable graphene sheets with high structural integrity, by simultaneously oxidising and ultrasonating (oxidi-sonication) commercial graphite particles. This technique is far more efficient than the currently used liquid exfoliation method, with the yield of single and few-layer graphene ranging 70–80 wt%. The as-prepared graphene sheets have thicknesses mainly 1–3 nm, which can suspend in acetone for at least 48 hours. Their C/O ratio is 8.85 and Raman I_D/I_G is 0.211, corresponding to an electrical conductivity of over 600 S/cm. These unique properties enabled the fabrication of transparent conductive films by casting. The film thicknesses can be readily controlled by tuning the volume of graphene suspension. Our synthesis method would promote the development of large-area thin films, paper-like membrane with controllable permeability, anisotropic ionic conductors and supercapacitors.

Acknowledgements

The authors thank the financial support by Australian Research Council (LP140100605). JM thanks Asbury for providing graphite, and appreciates lab support by J Toshach.

- 14 I. Zaman, H. C. Kuan, Q. Meng, A. Michelmoro, N. Kawashima, T. Pitt, L. Zhang, S. Gouda, L. Luong and J. Ma, *Adv. Funct. Mater.*, 2012, **22**, 2735–2743.
- 15 I. Zaman, T. T. Phan, H. C. Kuan, Q. Meng, L. T. Bao La, L. Luong, O. Youssf and J. Ma, *Polymer*, 2011, **52**, 1603–1611.
- 16 D. C. Marcano, D. V. Kosynkin, J. M. Berlin, A. Sinitskii, Z. Sun, A. Slesarev, L. B. Alemany, W. Lu and J. M. Tour, *ACS Nano*, 2010, **4**, 4806–4814.
- 17 D. R. Dreyer, S. Park, C. W. Bielawski and R. S. Ruoff, *Chem. Soc. Rev.*, 2010, **39**, 228–240.
- 18 K. Parvez, R. Li, S. R. Punireddi, Y. Hernandez, F. Hinkel, S. Wang, X. Feng and K. Müllen, *ACS Nano*, 2013, **7**, 3598–3606.
- 19 P. M. Ajayan and B. I. Yakobson, *Nature*, 2006, **441**, 818–819.
- 20 Y. Hernandez, V. Nicolosi, M. Lotya, F. M. Blighe, Z. Sun, S. De, I. McGovern, B. Holland, M. Byrne and Y. K. Gun'Ko, *Nat. Nanotechnol.*, 2008, **3**, 563–568.
- 21 J. C. Meyer, A. K. Geim, M. I. Katsnelson, K. S. Novoselov, T. J. Booth and S. Roth, *Nature*, 2007, **446**, 60–63.
- 22 W. Du, J. Lu, P. Sun, Y. Zhu, X. Jiang, *Chem. Phys. Lett.*, 2013, **568–569**, 198–201.
- 23 C. R. Herron, K. S. Coleman, R. S. Edwards and B. G. Mendis, *J. Mater. Chem.*, 2011, **21**, 3378–3383.
- 24 G. Wang, J. Yang, J. Park, X. Gou, B. Wang, H. Liu and J. Yao, *J. Phy. Chem C*, 2008, **112**, 8192–8195.
- 25 H. Chen, M. B. Müller, K. J. Gilmore, G. G. Wallace and D. Li, *Adv. Mater.*, 2008, **20**, 3557–3561.
- 26 C. Cheng and D. Li, *Adv. Mater.*, 2013, **25**, 13–30.
- 27 M. Fang, K. Wang, H. Lu, Y. Yang and S. Nutt, *J. Mater. Chem.*, 2010, **20**, 1982–1992.
- 28 A. C. Ferrari and D. M. Basko, *Nat Nano*, 2013, **8**, 235–246.
- 29 S. C. O'Hern, M. S. H. Boutilier, J. C. Idrobo, Y. Song, J. Kong, T. Laoui, M. Atieh and R. Karnik, *Nano. Lett.*, 2014.
- 30 Z. Luo, S. Kim, N. Kawamoto, A. M. Rappe and A. T. C. Johnson, *ACS Nano*, 2011, **5**, 9154–9160.
- 31 K. Liu, L. Liu, Y. Luo and D. Jia, *J. Mater. Chem.*, 2012, **22**, 20342–20352.
- 32 H. Zhu, P. Huang, L. Jing, T. Zuo, Y. Zhao and X. Gao, *J. Mater. Chem.*, 2012, **22**, 2063–2068.
- 33 S. Gadipelli, I. Calizo, J. Ford, G. Cheng, A. R. Hight Walker and T. Yildirim, *J. Mater. Chem.*, 2011, **21**, 16057–16065.
- 34 M. S. Dresselhaus, A. Jorio, M. Hofmann, G. Dresselhaus and R. Saito, *Nano. Lett.*, 2010, **10**, 751–758.
- 35 A. C. Ferrari, J. C. Meyer, V. Scardaci, C. Casiraghi, M. Lazzeri, F. Mauri, S. Piscanec, D. Jiang, K. S. Novoselov, S. Roth and A. K. Geim, *Phys. Rev. Lett.*, 2006, **97**, 187401.
- 36 L. M. Malard, M. A. Pimenta, G. Dresselhaus and M. S. Dresselhaus, *Physics Reports*, 2009, **473**, 51–87.
- 37 X. Li, W. Cai, J. An, S. Kim, J. Nah, D. Yang, R. Piner, A. Velamakanni, I. Jung, E. Tutuc, S. K. Banerjee, L. Colombo and R. S. Ruoff, *Science*, 2009, **324**, 1312–1314.
- 38 M. Wang, S. K. Jang, W. J. Jang, M. Kim, S. Y. Park, S. W. Kim, S. J. Kahng, J. Y. Choi, R. S. Ruoff, Y. J. Song and S. Lee, *Adv. Mater.*, 2013, **25**, 2746–2752.
- 39 M. Zhou, T. Lin, F. Huang, Y. Zhong, Z. Wang, Y. Tang, H. Bi, D. Wan and J. Lin, *Adv. Funct. Mater.*, 2013, **23**, 2263–2269.
- 40 M. Z. Iqbal, M. F. Khan, M. W. Iqbal and J. Eom, *J. Mater. Chem C*, 2014, **2**, 50404–5410.
- 41 H. C. Schniepp, J. L. Li, M. J. McAllister, H. Sai, M. Herrera-Alonso, D. H. Adamson, R. K. Prud'homme, R. Car, D. A. Saville and I. A. Aksay, *J. Phy. Chem B*, 2006, **110**, 8535–8539.
- 42 O. C. Compton, B. Jain, D. A. Dikin, A. Abouimrane, K. Amine and S. T. Nguyen, *ACS Nano*, 2011, **5**, 4380–4391.
- 43 A. F. Faria, D. S. T. Martinez, A. C. M. Moraes, M. E. H. Maia da Costa, E. B. Barros, A. G. Souza Filho, A. J. Paula and O. L. Alves, *Chem. Mater.*, 2012, **24**, 4080–4087.
- 44 I. Y. Jeon, D. Yu, S. Y. Bae, H. J. Choi, D. W. Chang, L. Dai and J. B. Baek, *Chem. Mater.*, 2011, **23**, 3987–3992.
- 45 C. K. Chua and M. Pumera, *J. Mater. Chem A*, 2013, **1**, 1892–1898.
- 46 S. M. Tan, A. Ambrosi, C. K. Chua and M. Pumera, *J. Mater. Chem A*, 2014, **2**, 10668–10675.
- 47 V. H. Pham, H. D. Pham, T. T. Dang, S. H. Hur, E. J. Kim, B. S. Kong, S. Kim and J. S. Chung, *J. Mater. Chem.*, 2012, **22**, 10530–10536.
- 48 C. Wu, X. Huang, G. Wang, L. Lv, G. Chen, G. Li and P. Jiang, *Adv. Funct. Mater.*, 2013, **23**, 506–513.
- 49 J. Shen, Y. Hu, M. Shi, X. Lu, C. Qin, C. Li, M. Ye, and M. Ye, *Chem. Mater.*, 2009, **21**, 3514–3520.
- 50 B. H. Wee and J. D. Hong, *Adv. Funct. Mater.*, 2013, **23**, 4657–4666.
- 51 S. Dubin, S. Gilje, K. Wang, V. C. Tung, K. Cha, A. S. Hall, J. Farrar, R. Varshneya, Y. Yang and R. B. Kaner, *ACS Nano*, 2010, **4**, 3845–3852.
- 52 O. C. Compton, D. A. Dikin, K. W. Putz, L. C. Brinson and S. T. Nguyen, *Adv. Mater.*, 2010, **22**, 892–896.
- 53 J. U. Lee, W. Lee, J. W. Yi, S. S. Yoon, S. B. Lee, B. M. Jung, B. S. Kim and J. H. Byun, *J. Mater. Chem A*, 2013, **1**, 12893–12899.
- 54 E. Kymakis, K. Savva, M. M. Stylianakis, C. Fotakis and E. Stratakis, *Adv. Funct. Mater.*, 2013, **23**, 2742–2749.
- 55 R. R. Nair, P. Blake, A. N. Grigorenko, K. S. Novoselov, T. J. Booth, T. Stauber, N. M. R. Peres and A. K. Geim, *Science*, 2008, **320**, 1308.
- 56 W. Du, X. Jiang, L. Zhu, *J. Mater Chem A*, 2013, **1**, 10592–10606.
- 57 C. G. Navarro, R. T. Weitz, A. M. Bittner, M. Scolari, A. Mews, M. Burghard and K. Kern, *Nano. Lett.*, 2007, **7**, 3499–3503.
- 58 K. Rana, J. Singh and J. H. Ahn, *J. Mater. Chem C*, 2014, **2**, 2646–2656.
- 59 Z. Wei, D. Wang, S. Kim, S. Y. Kim, Y. Hu, M. K. Yakes, A. R. Laracuente, Z. Dai, S. R. Marder, C. Berger, W. P. King, W. A. de Heer, P. E. Sheehan and E. Riedo, *Science*, 2010, **328**, 1373–1376.
- 60 J. Zhao, S. Pei, W. Ren, L. Gao and H. M. Cheng, *ACS Nano* 2010, **4**, 5245–5252.
61. Q. Zheng, W. H. Ip, X. Lin, N. Yousefi, K. K. Yeung, Z. Li and J. K. Kim, *ACS Nano* 2011, **5**, 6039–6051.
62. Q. Zheng, Z. Li, J. Yang and J. K. Kim, *Prog. Mater. Sci.*, 2014, **64**, 200–247.